RGNZ/MGPB

Hybrid Luus–Jaakola and Levenberg–Marquardt inversion for magnetic anomalies over 2D fault-like structures

Rudarsko-geološko-naftni zbornik
(The Mining-Geology-Petroleum Engineering Bulletin)
DOI: 10.17794/rgn.2026.4.7

Original scientific paper

CC BY

Mojtaba Babaei[1]*, Mohammad Rezaie[2]
[1] *Department of Geophysics, Ha.C., Islamic Azad University, Hamedan, Iran.*
[2] *Department of Mining Engineering, Faculty of Engineering, Malayer University, Malayer, Iran.*

Abstract
This study presents a shortened summary focusing on the hybrid Luus–Jaakola–Levenberg–Marquardt inversion and its superior performance on both synthetic and Perth Basin data.
In this study, a hybrid approach is introduced and evaluated for estimating the geometric and physical parameters of 2D fault structures from magnetic data. This method integrates the global search capability of the Luus–Jaakola (LJ) algorithm with the rapid convergence of the Levenberg–Marquardt (LM) algorithm, enhanced by two components: a multi-start strategy and a controlled perturbation scheme. This combination overcomes the limitations of initial value dependency and the instability of certain parameters, particularly the effective inclination angle (α). The performance of the proposed method was assessed using both synthetic and real-world data. The results demonstrate that the hybrid approach provides higher accuracy and stability in parameter estimation compared to each individual algorithm, especially under noisy conditions. Perturbation experiments and sensitivity analysis revealed a clear parameter hierarchy: depth parameters exhibit the strongest amplitude influence (approximately 200–267% variation), followed by the amplitude coefficient (approximately 85%) and the effective magnetization angle (approximately 63%), while the fault dip angle shows minimal amplitude sensitivity (approximately 5%). The analysis of the effective magnetization angle demonstrated its critical role in identifying optimal starting regions for stable estimations, with the location of these regions contingent on the state of other parameters. In the real-data application, the hybrid method yielded parameters consistent with plausible geological models of the area. The findings of this study offer a practical framework for improving magnetic data inversion, particularly in noise-contaminated environments.
In this study, a hybrid approach combining the Luus–Jaakola (LJ) and Levenberg–Marquardt (LM) algorithms is introduced for estimating the geometric and physical parameters of 2D fault structures from magnetic data. The method leverages the global search capability of LJ and the rapid convergence of LM, while incorporating a multi-start strategy and controlled perturbation to overcome initial value dependency and instability in critical parameters such as the effective inclination angle (α). The performance was assessed using both synthetic and real-world data. For synthetic data with 15% noise, the hybrid method achieved an RMS of 4.45 nT, significantly outperforming standalone LJ (17.44 nT) and LM (4.60 nT), while reducing the estimation error of α from 25.40% to 9.39% through controlled perturbation. When applied to real magnetic data from the Perth Basin, Australia, the hybrid approach yielded an RMS of 1.33 nT compared to 2.16 nT (LJ) and 10.61 nT (LM), producing parameters consistent with the plausible geological model of the area. These findings demonstrate that the hybrid framework offers superior accuracy and stability for magnetic data inversion, particularly under noisy conditions.

Keywords:
magnetic inversion; fault; Luus–Jaakola algorithm; Levenberg–Marquardt algorithm; hybrid Luus–Jaakola–Levenberg algorithm

1. Introduction

Magnetometry, a sub-discipline of exploration geophysics, enables the identification and modelling of subsurface structures by measuring variations in the Earth's magnetic field. These variations, known as "magnetic anomalies," arise from differences in the intensity and direction of magnetization in rocks and minerals. Magnetic bodies such as dikes, faults, or mineralized lenses disturb the ambient field, creating patterns with distinct amplitudes and shapes on the Earth's surface (**Sharma, 1987; Biswas and Acharya, 2016; Ekwok et al., 2023**).

Faults are fractures or shear zones within the Earth's crust along which significant displacement has occurred. This displacement alters the lithology and magnetic properties on either side of the fault, giving rise to a detectable magnetic anomaly. The primary objective of this research is to develop and apply an optimal method

* Corresponding author: Mojtaba Babaei
e-mail address: m_babaei@iau.ac.ir
Received: 16 October 2025. Accepted: 30 January 2026.
Available online: 21 July 2026

for estimating the geometric and physical parameters of a fault, including the amplitude coefficient, dip angle, effective magnetization angle, the depths to the top and bottom of the fault scarp, and the origin location, based on the analysis of these anomalies. The accurate interpretation of these parameters plays a crucial role in reconstructing the subsurface model, understanding tectonic processes, and exploration applications (**Grant and West, 1965**).

Numerous methods have been proposed for the interpretation of magnetic anomalies. These include least-squares methods (**Abdelrahman et al., 2009; Tlas and Asfahani, 2011**), Euler deconvolution (**Reid et al., 1990; Salem and Ravat, 2003; Dewangan et al., 2007**), Werner deconvolution (**Stagg et al., 1989; Hansen, 2005; Usman et al., 2014**), gradient methods (**Abdelrahman et al., 2007; Essa and Elhussein, 2017**), the analytic signal (**Nabighian, 1972; Salem, 2005; Aydin, 2008**), the tilt angle (**Miller and Singh, 1994; Essa et al., 2018; Pham et al., 2019; Elhussein and Shokry, 2020**), and the Fourier transform (**Gudmundsson, 1966; Gupta, 1988; Olurin et al., 2017**). Although these methods are simple and fast, they suffer from two fundamental limitations: high sensitivity to noise and dependency on initial information.

Gradient-based methods, such as the Levenberg–Marquardt (LM) algorithm (**Marquardt, 1963**), utilize the derivative of the objective function with respect to the parameters. Consequently, they exhibit rapid convergence and high precision near an optimal solution and require less computational memory. However, they are sensitive to the starting point, can face challenges with derivative computation in complex models, and are prone to becoming trapped in local minima, in addition to being sensitive to noise. In contrast, global search derivative-free methods, such as the Luus–Jaakola (LJ) algorithm (**Luus and Jaakola, 1973**), Genetic Algorithm (GA), Particle Swarm Optimization (PSO), Simulated Annealing (SA), Ant Colony Optimization (ACO), and Bat Algorithm (BA) (**Biswas and Acharya, 2016; Ekinci et al., 2019; Di Maio et al., 2020; Essa and Abo-Ezz, 2021; Essa, 2021; Singh and Biswas, 2021; Biswas et al., 2022; Ai et al., 2023; Babaei and Hosseini Pilangorgi, 2024; Babaei and Hosseini Pilangorgi, 2025**), are capable of exploring the entire parameter space and bypassing local minima. They are applicable even to complex nonlinear models without requiring derivatives. Nevertheless, compared to gradient-based methods, they suffer from slower convergence rates, the need for meticulous parameter tuning, and higher computational costs, while sensitivity to noise may persist under certain conditions.

The shared limitations of both classes of methods necessitate the development of a hybrid approach. Such a method would leverage the global search capability to eliminate dependency on the initial guess and avoid local minima, while simultaneously benefiting from the speed and accuracy of gradient-based techniques near the optimal solution. To this end, this study proposes a hybridization of the Luus–Jaakola global search algorithm with the Levenberg–Marquardt local optimization method. This combination is enhanced with two key components: a multi-start strategy and a controlled random perturbation scheme, aiming to improve the stability and accuracy of fault parameter estimation, particularly with noisy data. The results from applying this approach to both synthetic and real-world data indicate that the proposed hybrid method can recover all geological model parameters with high precision and completely eliminate the dependency on initial values. The remainder of this paper presents the mathematical framework and detailed implementation of the developed hybrid algorithm, the datasets and experimental conditions, the inversion results under various scenarios, and a comparative analysis with other conventional methods.

2. Materials and Methods

2.1. Luus–Jaakola Algorithm (LJ)

The Luus–Jaakola (LJ) algorithm is a derivative-free, stochastic direct search method employed for solving nonlinear optimization problems, particularly those involving complex or non-differentiable objective functions. Its core idea is to initiate a global search across the parameter space and then progressively shrink the search region to converge toward an optimal solution (**Luus and Jaakola, 1973**). In the context of parameter estimation, the objective function is defined as the Sum of Squared Errors (SSE), which is minimized:

$$S(X) = \min_{X} \sum_{i=1}^{m} \left(d_i^{\text{obs}} - d_i^{\text{calc}}(\text{X})\right)^2 \qquad (1)$$

where $\mathbf{X} = [x_1, x_2, \ldots, x_p]$ is the vector of p unknown model parameters, d_i^{obs} represents the i^{th} observed data point (from a total of m points), and d_i^{calc} is the corresponding model-calculated value for the parameter vector $\mathbf{X}$.

The algorithm commences by selecting initial values for the parameters, $\mathbf{X}^{(0)}$, an initial search radius, $\mathbf{r}^{(0)}$, for each parameter, and a shrinkage factor, ε. The shrinkage factor is a key component in the LJ method, controlling the size of the search domain. Initially, the search is performed over a large region of the parameter space. After each iteration, the dimensions of this region are reduced using the shrinkage factor. This contraction facilitates the gradual convergence of the search toward an optimal point. The value of ε is typically chosen between 0.85 and 0.95 to ensure a balance between reducing the search space and preventing a premature loss of sample diversity.

In each iteration j, a set of N candidate solutions is generated by perturbing the current best solution, $\text{X}^{(j)}$.

For each parameter x_i in the vector, a random number u_i is drawn from a uniform distribution over $[-1,1]$, and a new potential parameter value is calculated as:

$$x_{i,\text{candidate}}^{(j)} = x_i^{(j)} + u_i \cdot r_i^{(j)} \quad (2)$$

The objective function $S(\boldsymbol{X})$ is then evaluated for each of the N new candidate vectors. The candidate vector that yields the lowest objective function value becomes the new best solution for the next iteration, $\boldsymbol{X}^{(j+1)}$. Subsequently, the search radius is systematically reduced according to the rule:

$$r_i^{(j+1)} = \varepsilon \cdot r_i^{(j)} \quad (3)$$

This gradual reduction transitions the algorithm from a global exploration phase to a focused local exploitation phase. The process continues until a predefined maximum number of iterations, $j^{\max}$, is reached, or until the change in the objective function value falls below a convergence threshold. The defining features of the LJ algorithm are its ability to search a broad parameter space, its robustness against local minima, and its independence from derivative or Jacobian matrix computations.

2.2. Levenberg–Marquardt (LM) Algorithm

The Levenberg–Marquardt (LM) algorithm is a local nonlinear optimization method based on nonlinear least squares. It synergistically combines the advantages of the Gauss–Newton method and the gradient descent method. This algorithm is particularly effective for problems where the objective function has a complex curvature and high precision is required in the vicinity of the minimum (**Marquardt, 1963**). The LM objective function is also defined to minimize the sum of squared residuals between observed and calculated magnetic data. At each step, the LM algorithm provides an improved estimate of the required parameter adjustments by computing the gradient and the Jacobian matrix, **J**. The parameter update rule is given by (**Marquardt, 1963**):

$$\mathrm{X}^{(k+1)} = \mathrm{X}^{(k)} - (\mathrm{J}^T\mathrm{J} + \lambda\mathrm{I})^{-1}\mathrm{J}^T\mathrm{r} \quad (4)$$

where $\boldsymbol{X}^{(k)}$ is the parameter vector at iteration k, **J** is the Jacobian matrix of model sensitivities with respect to the parameters, **r** is the vector of residuals (ϕ^{obs} -ϕ^{calc}), **I** is the identity matrix, and λ is the damping factor. The damping factor interpolates between the Gauss–Newton method (as λ→0) and the gradient descent method (as λ→ ∞).

2.3. The Proposed Hybrid LJ-LM Method

The primary goal of this research is to estimate the model parameters including the amplitude coefficient (K), dip angle (θ), effective magnetization angle (α), depths to the top and bottom of the fault scarp (z_1 and z_2), and horizontal location (w) – by minimizing the misfit between the calculated magnetic data (T^{calc}) and the observed data (T^{obs}) as defined in **Equation 1**. To achieve this, we first implement the Luus–Jaakola (LJ) algorithm using a multi-start and perturbation strategy. This initial step is designed to generate multiple high-quality starting points for the subsequent local optimization.

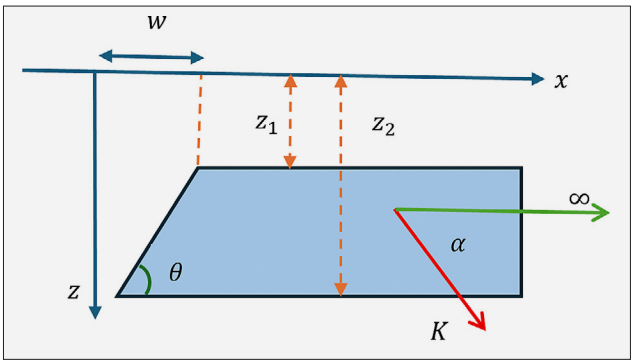


Figure 1: Inclined fault model

The Levenberg–Marquardt (LM) algorithm is then employed to refine the solutions obtained from the LJ phase. The key advantage of using LM in this context is its ability to converge rapidly to a precise solution when initiated near the global minimum. By seeding the LM algorithm with the high-quality initial guesses provided by the robust global search of LJ, the overall accuracy and stability of the inversion process for the studied magnetic anomalies are significantly enhanced.

3. Forward Model

In the forward modelling of a 2D fault, the total magnetic field anomaly, T_0, measured at a point x_i along a profile is considered to be composed of two components: a regional field, $Z(x_i)$, and the residual anomaly, $T(x_i)$ caused by the fault structure:

$$T_0(x_i) = T(x_i) + Z(x_i) \quad (5)$$

In this study, the residual anomaly is generated by a dipping fault model. The calculation of this anomaly is performed using the following forward model expression (**Aydin, 2008**):

$$T(x_i) = K\left\{\cos(\theta+\alpha)\left[tan^{-1}\left(\frac{(x_i-w)-(z_2-z_1)cot\alpha}{z_2}\right) - tan^{-1}\left(\frac{(x_i-w)}{z_1}\right)\right] + \sin(\theta+\alpha)\left[\ln\left(\frac{\left((x_i-w)-(z_2-z_1)cot\alpha\right)^2+{z_2}^2}{(x_i-w)^2+{z_1}^2}\right)^{1/2}\right]\right\} \quad (6)$$

In this model, the parameters are defined as follows (see also **Figure 1**):

- K is the amplitude coefficient (in nanoTeslas, nT),
- θ is the dip angle of the fault,

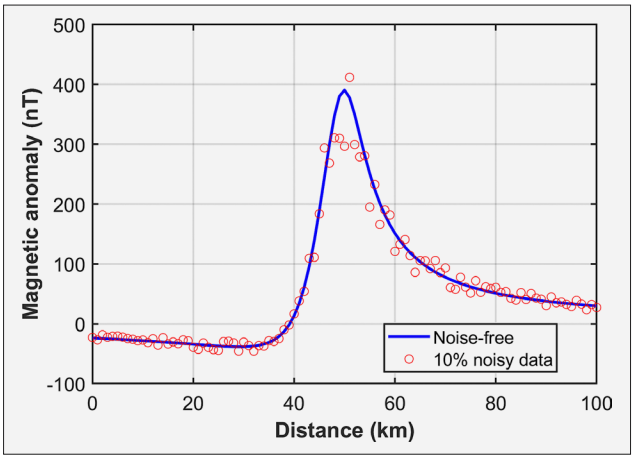


Figure 2: Synthetic magnetic anomaly calculated from the forward model (**Equation 6**) using true parameters K=400 nT, θ=35°, α=30°, z_1=4 km, z_2=7 km, w=50 km. Red line: noise-free model response; black circles: data with 10% random noise added according to **Equation 7**.

- α is the effective angle of magnetization,
- z_1 is the depth to the top edge of the fault,
- z_2 is the depth to the bottom edge of the fault,
- w is the horizontal location of the fault's origin along the profile.

The variable x_i represents the horizontal position of the observation point.

This equation describes the magnetic response of a 2D fault at any given observation point. It forms the basis for the comparison between modeled data and observed data during the inversion process.

4. Modelling (Synthetic Data)

To evaluate the proposed hybrid method, a synthetic magnetic anomaly dataset was generated based on the analytical model of a 2D dipping fault using **Equation 7**. First, the forward model response was calculated using the true parameters: . Subsequently, to simulate realistic conditions, 10% random noise from a uniform distribution was added to the data according to **Equation 7**:

$$T^{\text{Noisy}}(x_i) = T^{\text{True}}(x_i) \times [1 + \lambda \cdot (r_i - 0.5)] \qquad (7)$$

To examine the effect of noise, **Figure 2** displays the synthetic magnetic anomaly calculated from the forward model both with and without noise.

To analyze the results of the sensitivity analysis, the plots in **Figure 3** illustrate the changes in the model response due to a relative change in each parameter at three levels: 70%, 100% (the reference curve or base value), and 130% of the base value.

In these plots, the reference curve (100%) represents the original model state, against which the other curves are compared. A detailed interpretation of the sensitivity analysis is as follows:

- **Depth Parameters (z_1 and z_2)**: z_1 (see **Figure 3c**): Shows the classical burial depth effect. Shallower faults (70% = 2.8 km) produce stronger anomalies (~600 nT peak), while deeper faults (130% = 5.2 km) yield weaker signals (~200 nT peak). This behaviour reflects the well-known inverse relationship between source depth and anomaly amplitude. z_2 (see **Figure 3d**): Exhibits a seemingly counterintuitive pattern where increasing z_2 from 70% (4.9 km) to 130% (9.1 km) increases amplitude from ~150 nT to ~550 nT. This occurs because z_1 is held fixed (z_1 = 4 km) during the OAT analysis. Consequently, varying z_2 effectively changes the fault thickness (z_2 - z_1) from 0.9 km (at 70%) to 5.1 km (at 130%), with thicker faults naturally producing larger anomalies. This behaviour highlights an important distinction: while z_1 tests burial depth sensitivity (source-to-observer distance), z_2 in an One-At-a-Time (OAT) framework tests thickness sensitivity when z_1 is fixed. This is consistent with the standard practice of treating z_1 and z_2 as independent parameters during inversion, as both must be estimated separately to define the fault geometry completely. Both depth parameters significantly influence anomaly amplitude, with z_2 showing the highest overall sensitivity (267% amplitude variation) among all tested parameters.
- **Angular Parameters** (θ and α): The dip angle (θ) exhibits the expected inverse relationship with amplitude: steeper faults (larger θ) produce weaker anomalies due to reduced effective cross-sectional area. Over the tested range (24.5° to 45.5°), amplitude varies by approximately 5% (410 → 390 nT), indicating low amplitude sensitivity. The primary effect of θ is on anomaly shape and horizontal positioning rather than magnitude. The magnetization direction (α) predominantly controls the dipole asymmetry pattern but also moderately influences amplitude (~63% variation over ±30% parameter change) due to its trigonometric coupling in **Equation 6**, where it modulates both horizontal and vertical magnetic field components. While both angular parameters primarily affect anomaly shape, α shows notably higher amplitude sensitivity than θ.
- **Amplitude and Location Parameters** (K and w): Changes in the amplitude coefficient K produce significant amplitude variations (~85% over ±30% parameter change: 280 → 520 nT), demonstrating considerable model sensitivity. The horizontal location parameter w does not affect amplitude but controls the spatial positioning of the anomaly, its variation causes lateral displacement of the entire curve, which is a geometric translation rather than a sensitivity to anomaly intensity.

In summary, the OAT sensitivity analysis reveals a clear hierarchy: depth parameters (z_1, z_2) exhibit the strongest amplitude influence (~200–267% variation),

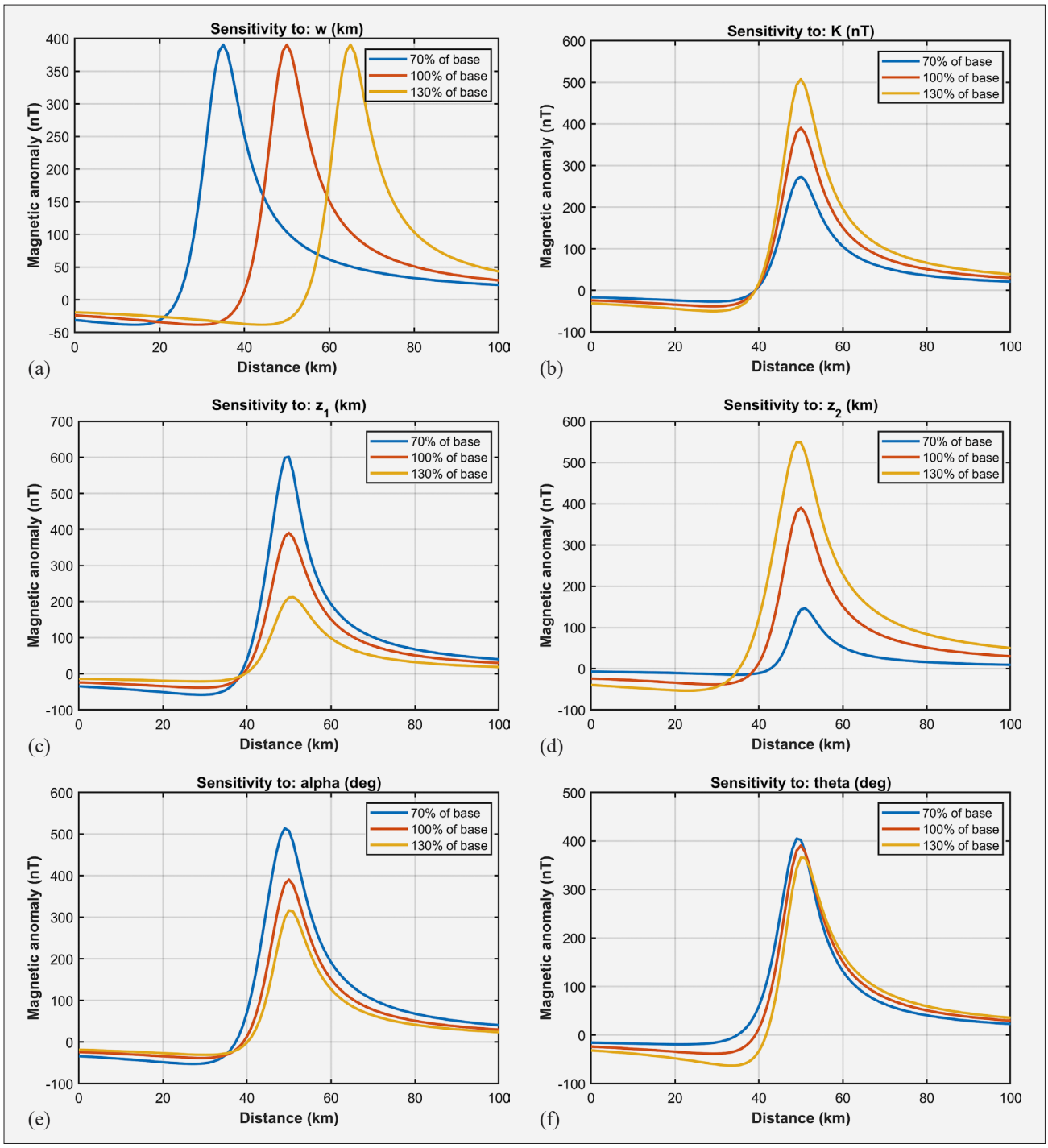


Figure 3: Sensitivity analysis showing changes in model response due to relative parameter variations at three levels: 70%, 100% (reference/base value), and 130% of base values. Panels show sensitivity to: (a) horizontal location w, (b) amplitude coefficient K, (c) depth to top edge z_1, (d) depth to bottom edge z_2, (e) effective magnetization angle α, and (f) fault dip angle θ. Results indicate K and θ have the most substantial impact on model response, while α exhibits the lowest sensitivity."

followed by K (~85%) and α (~63%), while θ shows minimal amplitude sensitivity (~5%). This ranking has direct implications for inversion: the high sensitivity of z_1, z_2, and K ensures robust parameter recovery, whereas the low amplitude sensitivity of θ – coupled with its strong shape influence – necessitates careful initialization, making it a critical focus for the hybrid LJ-LM approach.

5. Inversion of Synthetic Data

To assess the accuracy, stability, and efficiency of the inversion algorithms, a controlled synthetic dataset was initially employed. This approach facilitates the evaluation of the methods under ideal and reproducible conditions, where confounding factors such as measurement

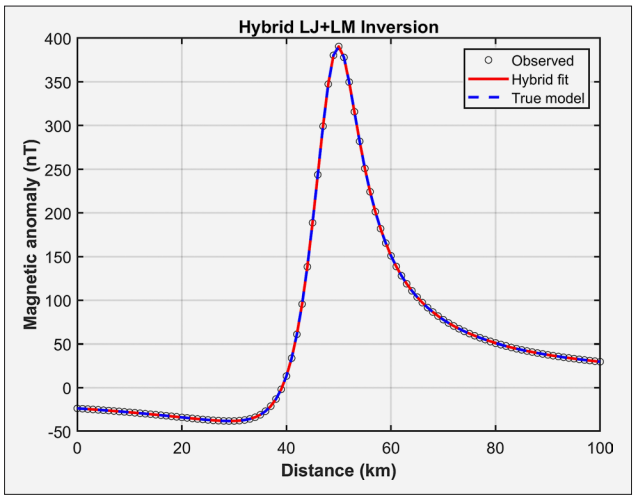


Figure 4: Comparison of observed magnetic anomaly (black circles) with hybrid LJ→LM inversion results (red line) for noise-free synthetic data. Dashed blue line: true model response. The hybrid method achieved perfect parameter recovery with RMS = 0.00 nT (see **Table 1**).

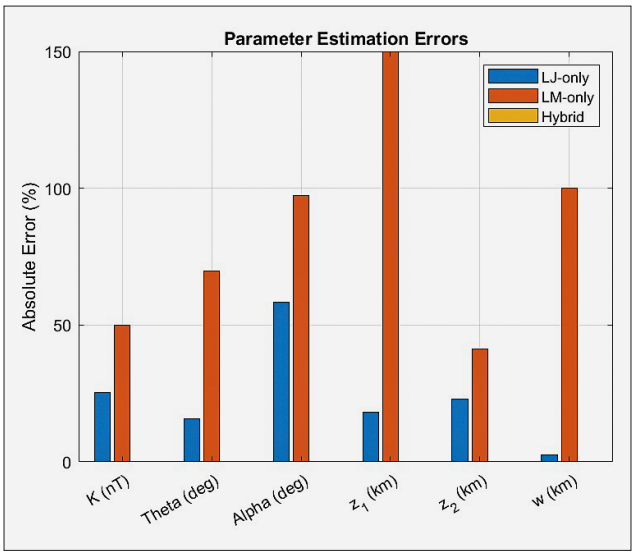


Figure 5: Comparison of the absolute percentage error in parameter estimation for the three inversion methods on noise-free data.

Table 1: True model parameter values and the estimated values from the three inversion methods for noise-free data, along with the percentage error and the Root Mean Square (RMS) error for each method.

Parameter	TRUE	LJ-only	%Err-LJ	LM-only	%Err-LM	Hybrid	%Err-HY
K (nT)	400.00	501.43	25.36	599.38	49.85	400.00	0.00
θ (°)	35.00	40.54	15.84	59.38	69.66	35.00	0.00
α (°)	30.00	47.54	58.45	0.81	97.29	30.00	0.00
z_1 (km)	4.00	4.73	18.27	10.00	150.00	4.00	0.00
z_2 (km)	7.00	8.60	22.87	9.90	41.38	7.00	0.00
RMS (nT)	–	11.23	–	105.24	–	0.00	–

noise or geological instabilities are eliminated. Consequently, the intrinsic capability of the algorithms to retrieve the true model parameters can be rigorously tested. The use of synthetic data also enables an objective comparison between different methods and allows for a detailed analysis of the model's sensitivity to initial parameter estimates and perturbations. In this section, the inversion results for noise-free data are first presented and compared. Subsequently, the same analyses are repeated using data contaminated with 10% peak-to-peak random noise to investigate the performance of the methods under conditions that more closely approximate real-world data.

5.1. Inversion Setup and Parameterization

To evaluate the performance of the algorithms, a synthetic magnetic anomaly dataset was generated using the true model parameters: $[K, \theta, \alpha, z_1, z_2, w] = [400\ \text{nT}, 35°, 30°, 4\ \text{km}, 7\ \text{km}, 50\ \text{km}]$. To robustly test the efficacy of the proposed hybrid method, the initial search bounds for the parameters were deliberately set to be wide. This was designed to challenge the standalone Levenberg–Marquardt algorithm, which is likely to face convergence issues under such conditions, thereby highlighting the ability of the hybrid method to overcome this challenge. The initial search ranges for the parameters were defined as follows:

- $K \in [200,600]$nT
- $\theta \in [1°, 90°]$
- $\alpha \in [1°, 90°]$
- $z_1 \in [1,10]$km
- $z_2 \in [1,100]$km
- $w \in [10,150]$km

Three distinct approaches were employed for parameter estimation:

1. **Luus–Jaakola (LJ) Method**: A global search configured with a maximum of 1000 iterations, an initial population of 50 candidates, and a shrinkage factor of 0.85.
2. **Levenberg–Marquardt (LM) Method**: A local optimization initiated with a random starting point selected from within the defined parameter bounds.
3. **Hybrid (LJ-LM) Method**: Execution of the LJ algorithm first, followed by using its best-fit output as the starting point for the LM algorithm to refine the solution.

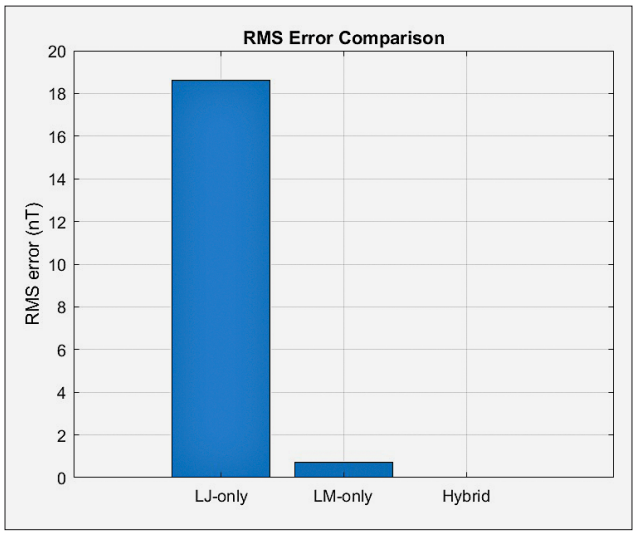


Figure 6: Comparison of the RMS error obtained from the three inversion methods for noise-free synthetic data.

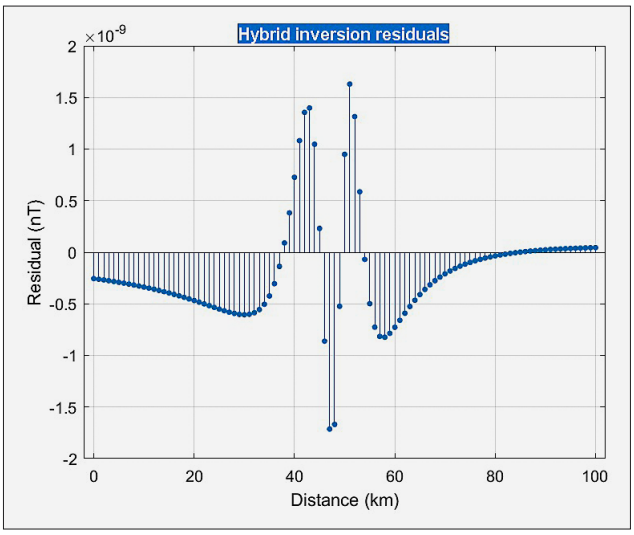


Figure 7: Residuals from the hybrid LJ→LM inversion for noise-free data.

5.2. *Initial Inversion Results (Noise-Free Data)*

To evaluate the performance of the proposed hybrid approach, which combines the Luus–Jaakola (LJ) global search algorithm with Levenberg–Marquardt (LM) local optimization, the synthetic data generated from the reference model were first inverted without the addition of measurement noise. **Figure 4** compares the observed data from the model, the fit produced by the hybrid method, and the response of the true model. As illustrated, the hybrid method successfully reproduced the observed anomaly curve completely, achieving a perfect match with the true model.

Table 1 presents the true parameter values alongside the values estimated by the standalone LJ algorithm, the standalone LM algorithm (initiated from the same random starting model), and the hybrid method. The table also includes the percentage error for each method.

As observed, the hybrid method was able to retrieve all parameters with perfect accuracy (zero error) and reduce the RMS error to zero (to two decimal places). In contrast, the standalone LM method, due to its high sensitivity to initial conditions, exhibited significant deviations, particularly for the parameter α and the depth parameters, resulting in a very high RMS error (over 105 nT). The LJ method performed better than LM but still demonstrated lower accuracy compared to the hybrid approach, particularly for parameters with lower sensitivity such as θ and α, which are more prone to convergence issues in standalone methods. This test demonstrates that even in the absence of noise, using the LM algorithm alone with an inadequate initial model leads to a severe divergence of the results. In contrast, the combination of a global search and a local optimization is capable of overcoming the dependency on the initial guess to recover the exact solution. **Figure 5** visually represents the percentage error for each parameter across the different methods.

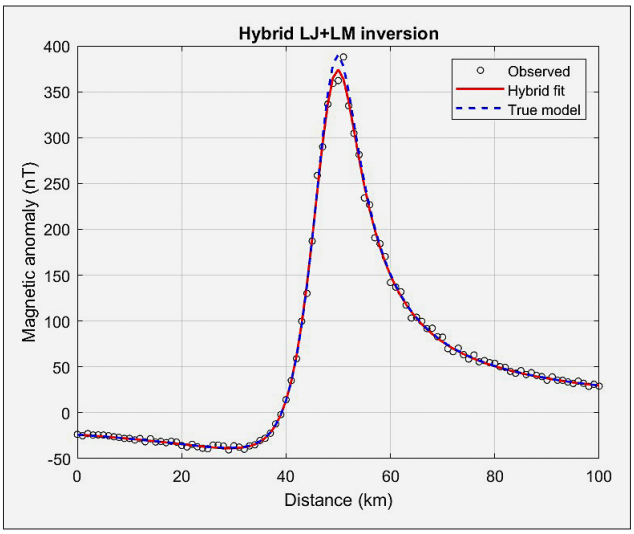


Figure 8: Comparison of 15% noisy synthetic magnetic data (black circles) with true model response (dashed blue line) and fit from hybrid LJ→LM method (solid red line). The hybrid method achieved RMS = 4.45 nT with parameter errors: K (1.96%), θ (1.29%), α (25.40%), z_1 (9.29%), z_2 (4.73%) as shown in **Table 2**.

As shown in **Figure 6**, the standalone LJ method recorded a notable RMS error (approximately 11.23 nT, as per Table 1). Although the standalone LM method achieved a much higher RMS (105.24 nT), the hybrid (LJ→LM) method successfully reduced the RMS error to virtually zero, indicating a complete reproduction of the model response and precise convergence in the absence of noise.

Figure 7 displays the residuals from the hybrid inversion, which have reached a magnitude on the order of 10^{-9}nT. This demonstrates a perfect fit between the model response and the observed data. The symmetrical distribution and extremely small amplitude of these residuals signify complete convergence and the high precision of the hybrid method in data reconstruction.

Table 2: Comparison of true and estimated model parameter values, percentage error, and RMS error for the 15% noisy data using the LJ, LM, and hybrid approaches.

Parameter	TRUE	LJ	%Err-LJ	LM	%Err-LM	Hybrid	%Err-HY
K (nT)	400.00	497.00	24.25	521.04	30.26	392.15	1.96
θ (°)	35.00	45.95	31.28	34.99	0.02	35.45	1.29
α (°)	30.00	47.20	57.34	21.71	27.62	22.38	25.40
z_1 (km)	4.00	4.94	23.48	4.82	20.56	4.37	9.29
z_2 (km)	7.00	8.81	25.92	6.51	6.96	6.67	4.73
RMS (nT)	---	17.44	---	4.60	---	4.45	---

5.3. *Inversion Results for Noisy Data*

To evaluate the stability of the algorithms against a higher level of noise, the synthetic data from the reference model were contaminated with 15% peak-to-peak random noise (relative to the signal's amplitude) and then inverted. All other conditions, including the parameter search ranges and the configuration of the three methods, remained identical to the previous sections. **Figure 8** illustrates the fit of the hybrid model to the 15% noisy data. The increased noise level led to greater dispersion in the observed data points and a reduction in the clarity of the signal's peak, creating more challenging conditions for achieving precise parameter convergence. Despite the evident scatter of the data points, the resulting fit still effectively reconstructs the overall signal trend and provides a suitable overlay, even in regions with high gradients.

Table 2 displays the true, estimated, and percentage error values for the parameters for each of the three methods under the 15% noise condition. As expected, the percentage errors have increased compared to the noise-free case. The parameter α exhibits the highest sensitivity to noise, with the errors for the standalone LJ and LM methods reaching approximately 57% and 28%, respectively. Nevertheless, the hybrid method successfully reduces the errors for all parameters and achieves the lowest RMS error (approximately 4.45 nT).

While the difference in RMS error between the standalone LM method (4.60 nT) and the hybrid LJ→LM approach (4.45 nT) may appear modest – only approximately 3% – the hybrid method demonstrates a substantially superior performance in parameter accuracy, particularly for the angular parameters. As shown in **Table 2** and **Figure 9**, the hybrid method achieves significantly lower percentage errors for nearly all parameters compared to both standalone methods. Most notably, for the critical parameter α (effective magnetization angle), the hybrid method reduces the error to 25.40%, compared to 27.62% for LM and 57.34% for LJ. Similarly, for the amplitude coefficient K and the dip angle θ, the hybrid method attains errors below 2%, whereas the standalone LJ method exhibits errors exceeding 24% and 31%, respectively. This demonstrates that the hybrid approach provides not only a slightly better data fit (lower RMS) but, more importantly, a more accurate and geologically meaningful parameter

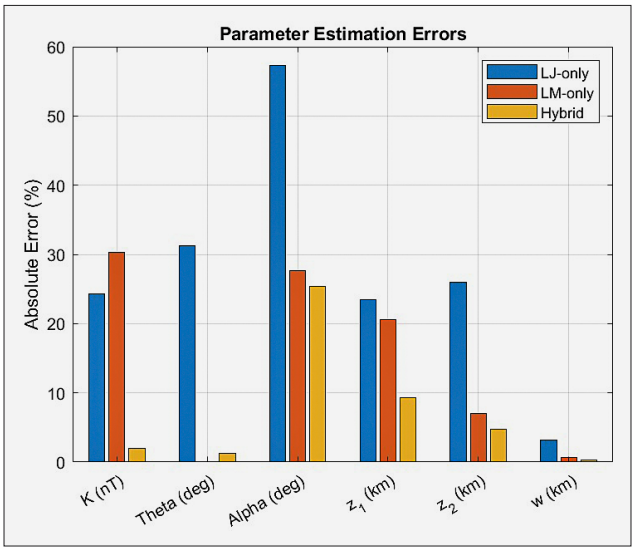


Figure 9: Absolute percentage error in parameter estimation for three inversion methods on 15% noisy synthetic data. LJ method shows highest errors (α > 57%), LM method shows improvement but still high error for α (≈28%), while hybrid method achieves lowest errors for nearly all parameters (< 3% for K and θ), demonstrating superior accuracy and stability under high-noise conditions.

estimation, which is the ultimate goal of geophysical inversion. The error distribution across parameters reflects the sensitivity hierarchy established in Section 4. The high-sensitivity parameters (z_1, z_2, K) converge more reliably even under noise, with the hybrid method achieving errors of 9.29% for z_1, 4.73% for z_2, and 1.96% for K. In contrast, α – despite its moderate-to-high sensitivity (~63%) – shows significantly higher error (25.40%) due to its trigonometric coupling in the forward model, which amplifies noise effects. The parameter θ, while showing low amplitude sensitivity (~5%), exhibits very low error (1.29%) in the hybrid approach, confirming that its strong shape influence allows stable convergence despite weak amplitude response.

Figure 9 illustrates the trend of absolute parameter errors for the three inversion approaches on the 15% noisy data. As can be seen, the LJ method recorded the highest error for all parameters. This error exceeds 57% for α, indicating its high sensitivity to noise. The LM method shows a significant improvement over LJ, yet it still exhibits a relatively high error for the α parameter (approxi-

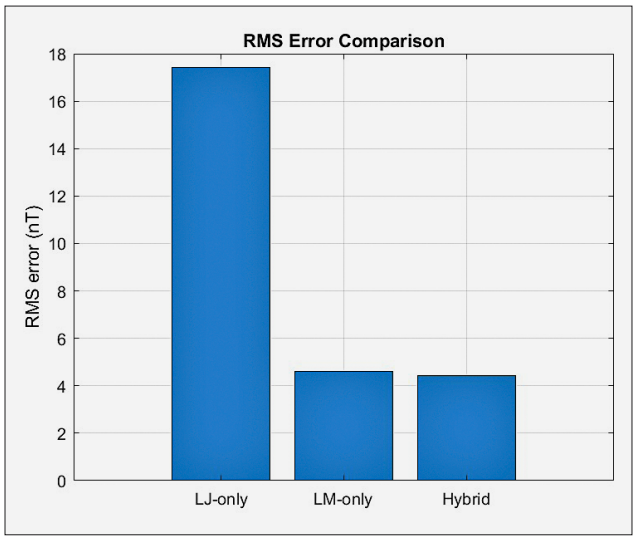


Figure 10: RMS error comparison for three inversion methods on 15% noisy synthetic data. Standalone LJ registered highest RMS (17.44 nT), indicating weaker convergence in noisy environment. Standalone LM and hybrid LJ→LM methods achieved considerably lower RMS values (4.60 nT and 4.45 nT respectively), demonstrating higher accuracy and greater robustness against noise.

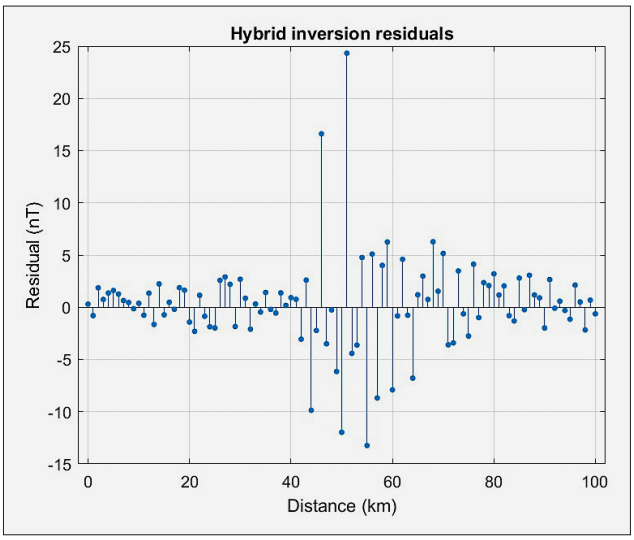


Figure 11: Residuals from hybrid LJ→LM inversion on 15% noisy synthetic data. The majority of residual values lie within ±5 nT range. Positive and negative spikes (up to approximately +24 nT and -14 nT) are direct consequence of noise perturbations. Overall symmetrical pattern around zero and absence of systematic trend indicate hybrid method reproduced model response with adequate fidelity.

mately 28%). In contrast, the hybrid method achieves the lowest error for nearly all parameters notably, less than 3% for K and θ which underscores its superior accuracy and stability even under high-noise conditions.

To better visualize the performance of the three inversion methods from an RMS error perspective, **Figure 10** presents a comparative bar chart of this metric for the 15% noisy data. As shown, the standalone LJ method registered the highest RMS value of 17.44 nT, indicating its weaker convergence in a noisy environment. The standalone LM and, particularly, the hybrid (LJ→LM) methods achieved considerably lower RMS values (4.60 nT and 4.45 nT, respectively), demonstrating their higher accuracy and greater robustness against noise.

Finally, **Figure 11** displays the residuals from the hybrid inversion. As can be observed, the majority of the residual values lie within the ±5 nT range. Only a few positive or negative spikes with larger amplitudes (up to approximately +24 nT and -14 nT) are visible, which are a direct consequence of the noise perturbations. The overall symmetrical pattern around zero and the absence of any systematic trend indicate that the hybrid method was able to reproduce the model response with adequate fidelity, even in the presence of relatively high noise.

6. Analysis and Interpretation of Algorithm Performance on Angular Parameters (α and θ)

The angular parameters of the model, comprising the effective dip (α) and the fault slope (θ), play a decisive role in shaping the magnetic anomaly and are typically challenging in terms of stability during the inversion process. Due to the model's nonlinear response to these parameters, the lower accuracy of local optimization methods, and their relatively high correlation with each other, these two parameters can cause algorithms to become trapped in local minima or yield estimates far from the true values.

To more thoroughly evaluate the performance of the three approaches standalone LJ, standalone LM, and the hybrid LJ→LM in estimating these two parameters, the effect of a controlled initial perturbation in α was first investigated to determine how the algorithms react to a change in the starting point. Subsequently, a two-dimensional α–θ sensitivity analysis was conducted to map the error distribution in the joint parameter space and identify its optimal region. The combination of these two tests provides a comprehensive picture of the algorithms' strengths and weaknesses and highlights the advantage of the hybrid method in selecting suitable starting points and achieving stable convergence.

6.1. Effect of a Controlled Initial Perturbation in α on the Performance of the Hybrid Algorithm

The results presented in the preceding sections demonstrated that the hybrid (LJ→LM) method consistently registered significantly lower RMS values compared to the standalone LJ or LM methods, for both noise-free and 15% noisy data. However, a closer examination of the absolute parameter error comparison figures reveals that all methods, including the hybrid one, exhibit weaker performance in estimating the parameter α (effective

Table 3: Comparison of inversion results for synthetic data with 15% noise after applying a perturbation of Δα = +7°.

Parameter	TRUE	LJ-only	%Err-LJ	LM-only	%Err-LM	Hybrid	%Err-HY
K (nT)	400.00	417.26	4.32	200.00	50.00	360.55	9.86
θ (°)	35.00	45.67	30.49	31.04	11.32	35.73	2.10
α (°)	30.00	47.99	59.96	11.21	62.63	27.18	9.39
z_1 (km)	4.00	4.93	23.23	10.00	150.00	4.28	6.94
z_2 (km)	7.00	8.82	26.06	1.25	82.08	6.76	3.40
RMS (nT)	---	13.94	---	84.58	---	4.44	---

dip) compared to other parameters. The model's nonlinear nature with respect to α, its high correlation with other angular parameters (especially θ), and its strong dependency on the starting point all contribute to local algorithms like LM easily becoming trapped in local minima or converging to inaccurate estimates.

Applying a controlled perturbation to the initial value of α can steer the search path toward more stable regions and increase the probability of escaping local minima. In this study, only the parameter α was displaced from its true value by an amount $\Delta\alpha$, such that $\alpha_{init} = \alpha_{true} + \Delta\alpha$. All other parameters were kept at their true values to isolate and purely evaluate the effect of the perturbation on α. The model response was then calculated with this new α value, and 15% peak-to-peak uniform random noise was added to the data. The inversion process was executed using all three algorithms: LJ, LM, and the hybrid LJ→LM. **Table 3** presents the estimated parameter values and their corresponding relative percentage errors for the unperturbed and initially perturbed α cases.

A comparison of these results indicates that for the hybrid method, applying a controlled perturbation led to a dramatic reduction in the error of α, from 25.40% (in **Table 2**) to 9.39%. This significant improvement was accompanied by relatively small changes in the other parameters; for instance, the percentage error decreased for parameters like θ and z_2, while it increased for others, including K. Another important observation is that the final RMS of the hybrid method remained nearly constant in both scenarios (4.45 nT → 4.44 nT), indicating that using a small, targeted perturbation preserved the overall quality of the fit without introducing negative side effects.

This finding, combined with the analysis of the figures showing the change in α error as a function of $\Delta\alpha$(see **Figure 12**), suggests that a limited range for the initial perturbation (around 1 to 2 degrees) can be optimal, providing the greatest error reduction. In contrast, larger perturbations (over 7 degrees) lead to a noticeable decline in accuracy. In summary, a small and targeted initial perturbation in α can be considered a form of guided local optimization that, while maintaining the overall fit quality, effectively compensates for this parameter's inherent weakness in stability and sensitivity to the starting point.

Figure 13 shows the relationship between the initial value of α and the estimated α after running the hybrid (LJ→LM) method on synthetic data with 15% noise. The horizontal axis represents the initial α value, obtained by adding the initial displacement $\Delta\alpha$ to the true value (30 degrees). The vertical axis displays the final estimated α after the inversion is complete. The black dashed line represents the initial value, the horizontal red line indicates the true value of α, and the colored points show the estimated values, with the color of each point corresponding to the final RMS value according to the color bar on the right. Points located above the red line indicate an overestimation, while proximity to it signifies higher accuracy. The plot demonstrates that for small perturbations, the estimated α remains close to the true value. However, as $\Delta\alpha$ increases, the estimates gradually deviate from the true value, with significant divergence occurring at larger perturbations (e.g. 8 to 10 degrees).

Although the plots in **Figures 12** and **13** were generated based on a specific scenario involving a 2D fault synthetic dataset with 15% noise and with other parameters held constant – and thus their results cannot be generalized as a universal rule for all models, noise conditions, or full inversion runs – their analysis provides several important insights for this particular problem. First, this sensitivity analysis shows that under controlled conditions, the minimum error for α occurs within a small initial perturbation range (approximately 1–2 degrees). Second, the curve in **Figure 12** reveals the existence of a "safe zone," which could be useful for tuning the initial value of α in this specific model and test data. Third, the rapid increase in error for perturbations exceeding about 7 degrees serves as a warning, highlighting the risk associated with choosing initial values far from reality. Thus, this case study, in addition to monitoring the sensitivity and stability of α, is valuable as a reference for comparison and for designing adaptive experiments under different geometric and noise conditions, although it should not be directly used as a guide for selecting initial values in real-world scenarios.

6.2. Two-Dimensional α–θ Sensitivity Analysis and its Relation to the Hybrid Results

To assess the model's sensitivity to key parameters, an RMS contour map was plotted in the α–θ space, while keeping the other parameters fixed at the values from the best hybrid solution (see **Figure 14**). The results show

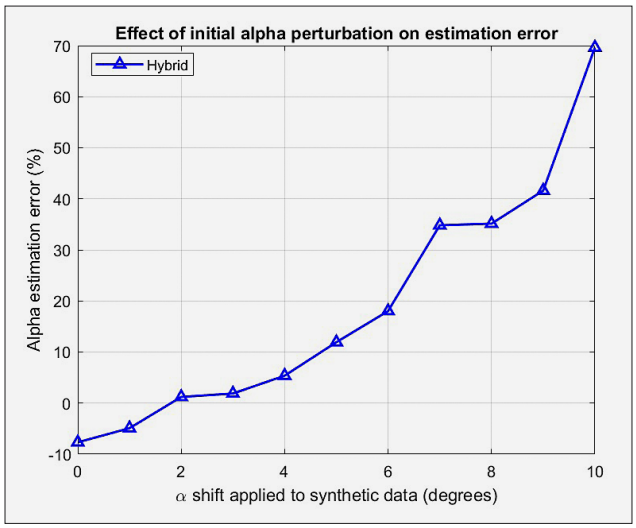


Figure 12: Variation of α estimation error in hybrid LJ→LM method as function of initial perturbation Δα for 15% noisy synthetic data. The analysis shows minimum error occurs within the small initial perturbation range (approximately 1–2 degrees). The rapid increase in error for perturbations exceeding about 7 degrees highlights the risk of choosing initial values far from reality.

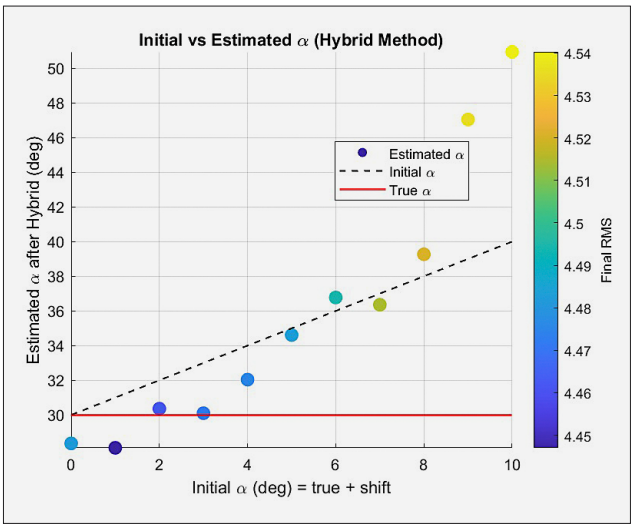


Figure 13: Estimated α from hybrid LJ→LM method versus initial α (true value of 30° plus Δα) for 15% noisy synthetic data. Black dashed line: initial value; horizontal red line: true α value; colored points: estimated values with color corresponding to final RMS. For small perturbations, estimated α remains close to true value. As Δα increases, estimates gradually deviate with significant divergence at larger perturbations (8-10 degrees).

that the region of minimum RMS is very narrow and is centered around $\alpha \approx 24°$ and $\theta \approx 35°$. This distribution indicates that small changes in these two parameters can cause significant variations in the model error. By comparing the values obtained from the hybrid method with the perturbed start ($\alpha = 27.18°, \theta = 35.73°$,RMS = = 4.44 nT) with the location of the contour minimum, it is observed that the θ value almost perfectly matches the optimal center, and the α value differs by only about 3°. This proximity demonstrates that the hybrid algorithm successfully entered the optimal error region and overcame the challenge of local minima traps.

7. Real Data Application: The Perth Basin Case Study, Australia

To assess the practical efficacy of the proposed magnetic inversion methods – namely the standalone LJ, standalone LM, and the hybrid LJ+LM approach – a real-world dataset from a magnetic anomaly profile over a fault structure on the western margin of the Perth Basin, Australia, was utilized. These data were first reported by **Qureshi and Nalaye (1978)** and have since been employed in several reputable geological and geophysical studies, including those by **Biswas and Rao (2021)** and **Essa et al. (2023)**. The profile has a total length of 40 km and was sampled at 1 km intervals (see **Figure 15**). This case validates the applicability of the 2D assumption because the selected profile represents a laterally homogeneous section, as consistently utilized in previous Perth Basin inversion studies (**Biswas and Rao, 2021; Essa et al., 2023**).

After digitizing the data, this profile served as the basis for the analysis and estimation of the fault model parameters in this study. The Perth Basin, located in Western Australia, has a north-south trend. It is considered the southern extension of the Carnarvon Basin and, with an area of approximately 100,000 km², is of significant geomorphological and economic importance. The presence of more than twenty commercial oil and gas fields underscores the region's significance in hydrocarbon exploration. The basin's formation resulted from an intracontinental rifting process that ultimately led to the separation of India from Australia, recording a thick succession of sediments from the Permian to the present day. Its tectonic and structural boundaries, particularly on the western side, host major fault systems and are considered prospective zones for mineral and energy resource exploration, making their study of considerable scientific and industrial value (**Olierook et al., 2015**).

In this research, the forward model (**Equation 6**) was used to simulate the magnetic response of the 2D fault, and the search bounds for the parameters were selected based on geological information and previous studies. First, the LJ algorithm was executed as a global search, followed by the LM algorithm for local refinement of the parameters. In the hybrid LJ+LM approach, to enhance the stability of the parameter α (effective dip), a small random perturbation ($\pm 1°$) was added to its value after the LJ run. A wider search margin of 0.20 was then applied for α in the subsequent LM search, while other parameters were searched within a standard margin of 0.10. This hybrid cycle was repeated over 10 runs with internal multi-starts to secure the lowest possible RMS minimum.

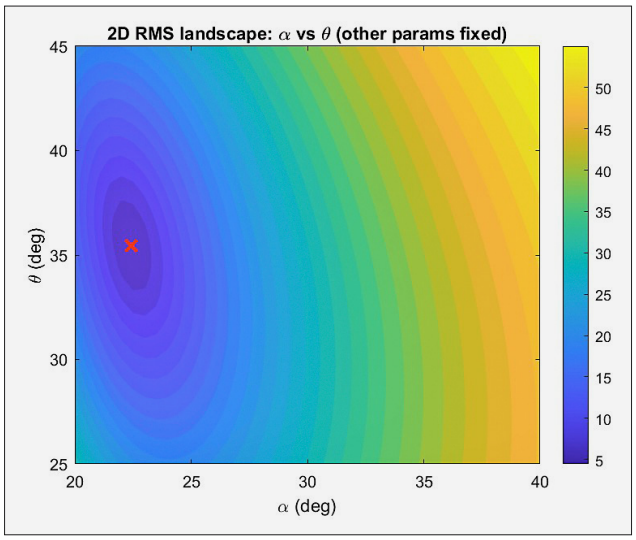


Figure 14: RMS contour map in α–θ parameter space with other parameters fixed at best hybrid solution values. The minimum RMS region is very narrow, centered around α≈24° and θ≈35°. The hybrid method with perturbed start (α=27.18°, θ=35.73°, RMS=4.44 nT) shows the θ value almost perfectly matches the optimal center, and α differs by only ~3°, demonstrating successful entry into optimal error region while overcoming local minima traps.

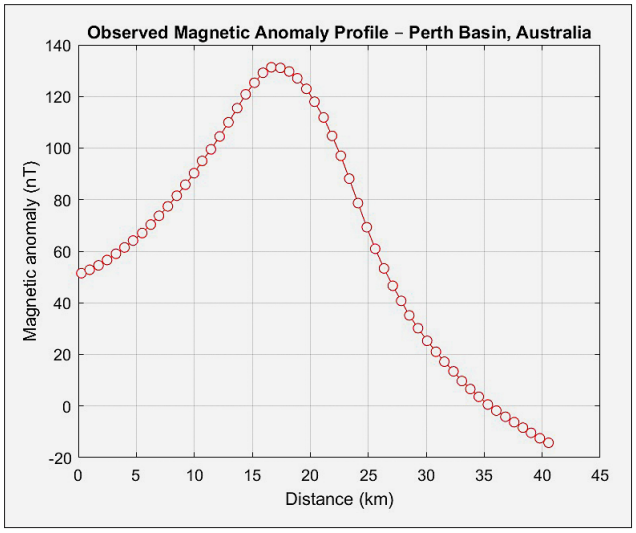
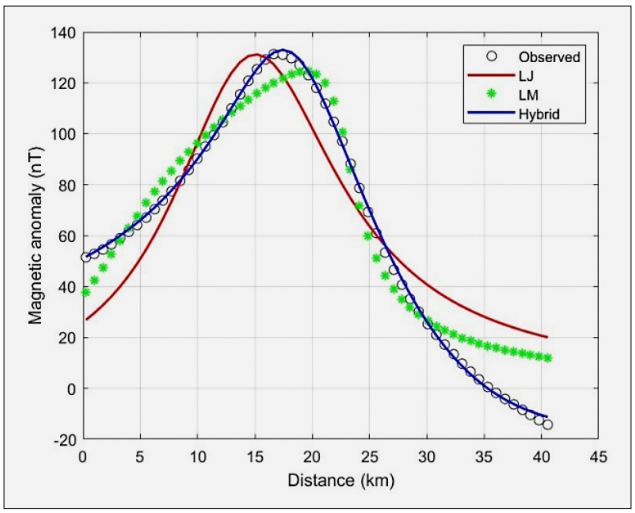


Figure 15: Observed magnetic anomaly profile over the western boundary of the Perth Basin, Australia.

To ensure the best possible outcome was achieved, a multi-run wrapper framework was also implemented. This framework executed the entire three-pronged process (LJ, LM, Hybrid) 50 times with different initial conditions, selecting and recording the best global result based on the lowest RMS achieved by the hybrid method.

Figure 16 illustrates the model fit to the real Perth Basin data. As can be observed, while the output of the LJ algorithm follows the general shape of the anomaly, it shows a significant discrepancy on the eastern flank of the curve (at distances greater than 30 km). The LM approach, initiated with random starts, provides a better local fit than



Figuer 16: Perth Basin real magnetic anomaly data (**Qureshi and Nalaye, 1978**) inverted using three methods. Black circles: observed data (40 km profile, 1 km sampling); red line: LJ method (RMS=2.16 nT); green stars: LM method (RMS=10.61 nT); blue line: hybrid LJ+LM with α perturbation and multi-start (RMS=1.33 nT). The hybrid method achieved lowest error, demonstrating superior performance on real fault structure data.

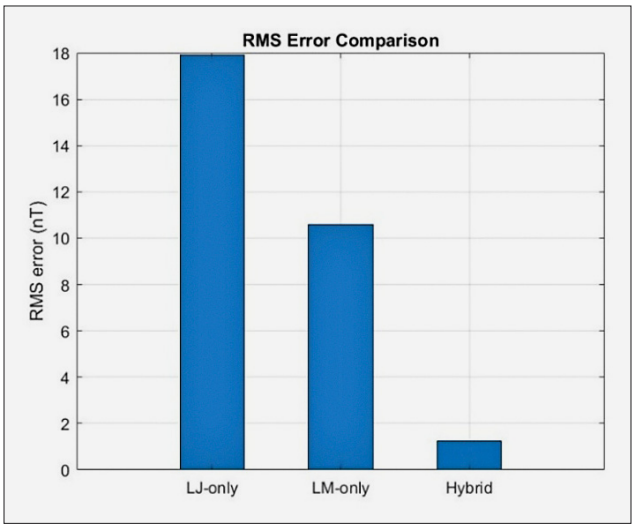


Figure 17: RMS error comparison for Perth Basin real data inversion. Hybrid LJ+LM method achieved lowest error (1.33 nT), performing significantly better than standalone LJ (2.16 nT) and LM (10.61 nT) methods, confirming practical efficacy of the proposed hybrid approach on real-world fault structures.

LJ but has limited accuracy around the anomaly's peak. In contrast, the hybrid LJ+LM method – implemented with an initial perturbation on α and a wider search margin for it – successfully reconstructed the curvature of the peak and the decay slope in the far-field regions, closely matching the observed data. It achieved the lowest RMS among the three approaches (see **Figure 17**). This result clearly demonstrates the superior agreement of the hybrid method with the real data and validates the choice of the stabilization settings for α in a real-world application.

Table 4: Estimated parameters for the 2D fault from real data using the hybrid (LJ→LM), standalone LJ, and standalone LM algorithms, compared with previous studies.

Parameter	LJ	LM	Hybrid	Essa (2023)	Qureshi & Nalaye (1978)	Rao & Babu (1983)	Tlas & Asfahani (2011)	Di Maio et al. (2020)
K (nT)	223.6	46.41	128	146.62	-	-	200.56	169.4
z_1 (km)	7.06	2.03	6.16	5.98	5.80–6.85	6.26	7.22	8.5
z_2 (km)	12.8	7.113	13.13	14.99	15.55–17	15.45	13.72	12
θ (°)	146.5	10	93.25	95.64	30	40	35.56	35.86
α (°)	-69.5	13.13	-21.45	-21.14	-	-	-	-
w (km)	19.79	22.79	17.9	18.05	-	-	-	-
RMS (nT)	2.163	10.61	1.33	7.18	-	-	-	-

Table 4 presents the quantitative results of the inversion process for the real Perth Basin data, alongside the findings from five key previous studies.

The consistency of our depth estimates with the range reported across multiple studies (z_1: 5.80–8.50 km, z_2: 12–17 km) and particularly close agreement with recent advanced methods (Essa et al., 2023) demonstrates the reliability of our hybrid approach. Moreover, our substantially lower RMS error (1.33 nT compared to 2.16–10.61 nT in other studies) indicates superior data fitting while maintaining geologically plausible parameters.

An analysis of the inversion results, as detailed in **Table 4**, highlights the superior performance of the proposed hybrid LJ-LM algorithm. The key findings are summarized as follows:

1. **Superior Data Fit**: The hybrid method achieved the lowest Root Mean Square (RMS) error of 1.33 nT. This value indicates a significantly better fit to the observed data compared to both the standalone LJ (RMS = 2.163 nT) and the standalone LM (RMS = 10.61 nT) algorithms. Notably, our method's RMS is also considerably lower than the 7.18 nT reported in the recent study by **Essa et al. (2023)**.
2. **Accurate Parameter Estimation**: The parameters estimated by the hybrid approach demonstrate strong geological consistency. The values for top depth ($z_1 = 6.16$ km), slope angle ($\theta = 93.25°$), effective magnetization inclination ($\alpha = -21.45°$), and horizontal position ($w = 17.9$ km) show excellent agreement with the findings of **Essa et al. (2023)**. Furthermore, the estimated top depth (z_1) falls precisely within the classic range of 5.80–6.85 km established by **Qureshi and Nalaye (1978)**.
3. **Limitations of Standalone Methods**: The standalone algorithms showed significant drawbacks. Although the LJ method produced a moderate RMS, it yielded a geologically implausible slope angle ($\theta = 146.5°$). Conversely, the LM method failed to converge to a meaningful solution, resulting in an extremely high RMS (10.61 nT) and inaccurate parameter estimates, which underscores its dependency on a good initial model.

In conclusion, the results from our hybrid model were compared with a wider range of studies (**Rao and Babu, 1983; Tlas and Asfahani, 2011; Di Maio et al., 2020**). This comparison shows that our model consistently aligns with established literature regarding the structure's key parameters, such as the amplitude factor (K) and depths (z_1, z_2).

While direct validation through gravity data or borehole information was not available for this study, the strong agreement of our results with six independent investigations using diverse optimization methods (see **Table 4**) provides compelling evidence for the accuracy of the estimated fault parameters. Future studies integrating multi-method geophysical data and detailed borehole information would further strengthen subsurface characterization in this region. Future Work: The methodology may be extended to 3D magnetic data and integrated airborne or geothermal exploration settings.

8. Conclusions

In this study, a hybrid approach was developed and evaluated for the inversion of magnetic anomalies caused by 2D fault structures. The method is based on the combination of the Luus–Jaakola (LJ) and Levenberg–Marquardt (LM) algorithms, enhanced with two key components: a multi-start strategy and a controlled perturbation technique. The primary objective was to overcome the limitation of initial model dependency and to improve the stability of estimating geometric and physical parameters, particularly the effective inclination angle, α.

The results from synthetic data demonstrated that the hybrid method achieves higher accuracy compared to standalone LJ and LM implementations. For instance, in the presence of 15% noise, our approach reduced the RMS error to 4.45 nT, a significant improvement over the values obtained from standalone LJ (17.44 nT) and LM (4.60 nT). Furthermore, by applying a suitable initial perturbation to α, its estimation error was successfully reduced from 25.40% to 9.39%. The one-dimensional analysis of Δα and the two-dimensional sensitivity analysis of the α-θ space confirmed that small perturba-

tion ranges can define "safe" starting regions for achieving more stable convergence, and that the optimal location of these regions depends on whether other parameters are fixed or free.

Importantly, these results reveal a critical distinction between data fit quality and parameter accuracy. While the standalone LM method achieved an RMS of 4.60 nT – close to the hybrid method's 4.45 nT – the hybrid approach delivered dramatically superior parameter recovery. The percentage errors for K and θ were reduced to less than 2% with the hybrid method, compared to 24-31% with LJ. This highlights a crucial point often overlooked in inversion studies: a good data fit (low RMS) does not necessarily guarantee an accurate parameter estimation, especially in highly nonlinear problems. The hybrid method's ability to combine global exploration with local refinement ensures both aspects are optimized simultaneously.

When applied to real data from the Perth Basin, Australia, the hybrid method again proved its superiority by achieving an RMS of 1.33 nT (compared to 2.16 nT for LJ and 10.61 nT for LM) and yielding parameters consistent with the plausible geological model of the area.

For the Perth Basin case study, the convergence of results from multiple optimization algorithms (see **Table 4**) effectively serves as indirect validation in the absence of direct ground-truth data. The estimated fault geometry, with depths of 6.16 km to 13.13 km and near-vertical dip (93.25°), is consistent with the tectonic setting of a rift basin margin. Collectively, the findings indicate that this hybrid approach provides an effective framework for enhancing the accuracy and stability of magnetic data inversion, especially under noisy conditions. It can therefore be employed as a practical and robust solution in similar geophysical investigations. The methodology shows particular promise for airborne magnetic surveys, mineral exploration in structurally complex areas, and geothermal fault detection.

9. References

Abdelrahman, E. M., Abo-Ezz, E. R., Essa, K. S., El-Araby, T. M., & Soliman, K. S. (2007). A new least-squares minimization approach to depth and shape determination from magnetic data. *Geophysical Prospecting*, *55*(4), 433–446.

Abdelrahman, E. M., Soliman, K. S., El-Araby, T. M., Abo-Ezz, E. R., & Essa, K. S. (2009). A least-squares standard deviation method to interpret magnetic anomalies due to thin dikes. *Near Surface Geophysics*, *7*(1), 41–46.

Ai, H., Ekinci, Y. L., Balkaya, Ç., & Essa, K. S. (2023). Inversion of geomagnetic anomalies caused by ore masses using Hunger Games Search algorithm. *Earth and Space Science*, *10*(8), e2023EA003002.

Aydin, I. (2008). Estimation of the location and depth parameters of 2D magnetic sources using analytical signals. *Journal of Geophysical Engineering*, *5*(3), 281–289.

Babaei, M., & Hosseini Pilangorgi, S. M. (2024). Estimation of conductive and non-conductive spherical geometrical parameters as a model of unexploded ordnance with electromagnetic induction data using genetic algorithm. *Iranian Journal of Geophysics*, *18*(5), 67–82.

Babaei, M., & Hosseini Pilangorgi, S. M. (2025). Estimation of layered earth conductivity with electromagnetic induction data in the low induction number range using the genetic algorithm method. *Journal of the Earth and Space Physics*, *51*(2), 289–307. https://doi.org/10.22059/jesphys.2025.385912.1007646

Biswas, A., & Acharya, T. (2016). A very fast simulated annealing method for inversion of magnetic anomaly over semi-infinite vertical rod-type structure. *Modeling Earth Systems and Environment*, *2*(4), 1–10.

Biswas, A., & Rao, K. (2021). Interpretation of magnetic anomalies over 2D fault and sheet-type mineralized structures using very fast simulated annealing global optimization: An understanding of uncertainty and geological implications. *Lithosphere*, *2021*(Special 6), 2964057.

Biswas, A., Rao, K., & Mondal, T. S. (2022). Inverse modeling and uncertainty assessment of magnetic data from 2D thick dipping dyke and application for mineral exploration. *Journal of Applied Geophysics*, 207, 104848.

Dewangan, P., Ramprasad, T., Ramana, M. V., Desa, M., & Shailaja, B. (2007). Automatic interpretation of magnetic data using Euler deconvolution with nonlinear background. *Pure and Applied Geophysics*, *164*(12), 2359–2372.

Di Maio, R., Milano, L., & Piegari, E. (2020). Modeling of magnetic anomalies generated by simple geological structures through Genetic-Price inversion algorithm. *Physics of the Earth and Planetary Interiors*, *305*, 106520.

Ekinci, Y. L., Balkaya, Ç., & Göktürkler, G. (2019). Parameter estimations from gravity and magnetic anomalies due to deep-seated faults: Differential evolution versus particle swarm optimization. *Turkish Journal of Earth Sciences*, *28*(6), 860–881.

Ekwok, S. E., Eldosouky, A. M., Essa, K. S., George, A. M., Abdelrahman, K., Fnais, M. S., Andráš, P., Akaerue, E. I., & Akpan, A. E. (2023). Particle swarm optimization (PSO) of high-quality magnetic data of the Obudu basement complex, Nigeria. *Minerals*, *13*(9), 1209.

Elhussein, M., & Shokry, M. (2020). Use of airborne magnetic data for edge basalt detection in Qaret Had El Bahr area, Northeastern Bahariya Oasis, Egypt. *Bulletin of Engineering Geology and the Environment*, *79*, 4483–4499.

Essa, K. S., & Elhussein, M. (2017). A new approach for the interpretation of magnetic data by a 2-D dipping dike. *Journal of Applied Geophysics*, *136*, 431–443.

Essa, K. S., Nady, A. G., Mostafa, M. S., & Elhussein, M. (2018). Implementation of potential field data to depict the structural lineaments of the Sinai Peninsula. *Journal of African Earth Sciences*, *147*, 43–53.

Essa, K. S. (2021). Evaluation of the parameters of fault-like geologic structure from the gravity anomalies applying the particle swarm. *Environmental Earth Sciences*, *80*, 489.

Essa, K. S., & Abo-Ezz, E. R. (2021). Potential field data interpretation to detect the parameters of buried geometries by applying a nonlinear least-squares approach. *Acta Geodaetica et Geophysica*, *56*(3), 387–406.

Essa, K. S., Abo-Ezz, E. R., Géraud, Y., Diraison, M., & Reid, A. B. (2023). Magnetic anomaly interpretation for 2D fault-like geologic structures utilizing the global particle swarm method. Journal of King Saud University – *Science*, 35, 102989.

Grant, F. S., & West, G. F. (1965). *Interpretation theory in applied geophysics*. New York, NY: McGraw-Hill Book Co.

Gudmundsson, G. (1966). Interpretation of one-dimensional magnetic anomalies by use of the Fourier transform. *Geophysical Journal of the Royal Astronomical Society*, *12*(1), 87–97.

Gupta, O. P. (1988). A Fourier transform minimization technique for interpreting magnetic anomalies of some two-dimensional bodies. *Canadian Journal of Exploration Geophysics*, *24*, 179–184.

Hansen, R. O. (2005). 3D multiple-source Werner deconvolution for magnetic data. *Geophysics*, *70*(4), L45–L51.

Luus, R., & Jaakola, T. H. I. (1973). Optimization by direct search and systematic reduction of the size of search region. *AIChE Journal*, *19*(4), 760–766.

Marquardt, D. W. (1963). An algorithm for least-squares estimation of nonlinear parameters. *Journal of the Society for Industrial and Applied Mathematics*, *11*(2), 431–441.

Miller, H. G., & Singh, V. (1994). Potential field tilt – a new concept for location of potential field sources. *Journal of Applied Geophysics*, *32*(2), 213–217.

Nabighian, M. N. (1972). The analytic signal of two-dimensional bodies with polygonal cross-section: Its properties and use for automated interpretation. *Geophysics*, *37*(3), 507–517.

Qureshi, I. R., & Nalaye, A. M. (1978). A method for the direct interpretation of magnetic anomalies caused by two-dimensional vertical faults. *Geophysics, 43*(1), 179–188.

Olierook, H. H., Timms, N. E., Wellmann, J. F., & others. (2015). 3D structural and stratigraphic model of the Perth Basin, Western Australia: Implications for subbasin evolution. *Australian Journal of Earth Sciences, 62*(4), 447–467.

Olurin, O. T., Ganiyu, S. A., Hammed, O. S., & Aluko, T. J. (2017). Interpretation of aeromagnetic data over Abeokuta and its environs, Southwest Nigeria, using spectral analysis (Fourier transform technique). *Materials and Geoenvironment*, *63*(3), 199–212.

Pham, L. T., Oksum, E., & Do, T. D. (2019). Edge enhancement of potential field data using the logistic function and the total horizontal gradient. *Acta Geodaetica et Geophysica*, *54*(2), 143–155.

Reid, A. B., Allsop, J. M., Granser, H., Millett, A. J., & Somerton, I. W. (1990). Magnetic interpretation in three dimensions using Euler deconvolution. *Geophysics*, *55*(1), 80–91.

Salem, A. (2005). Interpretation of magnetic data using analytic signal derivatives. *Geophysical Prospecting*, *53*(1), 75–82.

Salem, A., & Ravat, D. (2003). A combined analytic signal and Euler method (AN-EUL) for automatic interpretation of magnetic data. *Geophysics*, *68*(6), 1952–1961.

Sharma, P. V. (1987). Magnetic method applied to mineral exploration. *Ore Geology Reviews*, *2*(4), 323–357.

Singh, A., & Biswas, A. (2021). Global particle swarm optimization technique in the interpretation of residual magnetic anomalies due to simple geo-bodies with idealized structure. *Basics in Computational Geophysics*, *1*, 13–32.

Stagg, H. M. J., Wilcox, J. B., & Needham, D. J. L. (1989). Werner deconvolution of magnetic data: Theoretical models and application to the Great Australian Bight. *Australian Journal of Earth Sciences*, *36*(1), 109–122.

Tlas, M., & Asfahani, J. (2011). A new best-estimate methodology for determining magnetic parameters related to field anomalies produced by buried thin dikes and horizontal cylinder-like structures. *Pure and Applied Geophysics*, *168*(5), 861–870.

Usman, N., Lawal, K. M., & Aku, M. O. (2014). Application of Werner deconvolution method in the direct interpretation of residual aeromagnetic anomalies. *IOSR Journal of Applied Physics*, *6*(1), 18–21.

SAŽETAK

Hibridna Luus-Jaakolina i Levenberg-Marquardtova inverzija za magnetske anomalije nad 2D rasjednim strukturama

Ova studija predstavlja skraćeni sažetak usmjeren na hibridnu Luus-Jaakola-Levenberg-Marquardtovu inverziju i njezine iznimne performanse na sintetičkim podatcima i podatcima bazena Perth.
U ovoj studiji predstavljen je i evaluiran hibridni pristup za procjenu geometrijskih i fizičkih parametara 2D rasjednih struktura iz magnetskih podataka. Ova metoda integrira mogućnost globalnoga pretraživanja Luus-Jaakolina (LJ) algoritma s brzom konvergencijom Levenberg-Marquardtova (LM) algoritma, poboljšanu dvjema komponentama: strategijom višestrukoga pokretanja i shemom kontroliranih perturbacija. Ova kombinacija prevladava ograničenja ovisnosti početne vrijednosti i nestabilnosti određenih parametara, posebno efektivnoga kuta nagiba (α). Performanse predložene metode procijenjene su korištenjem sintetičkih i stvarnih podataka. Rezultati pokazuju da hibridni pristup pruža veću točnost i stabilnost u procjeni parametara u usporedbi sa svakim pojedinačnim algoritmom, posebno u uvjetima šuma. Eksperimenti perturbacije i analiza osjetljivosti otkrili su jasnu hijerarhiju parametara: parametri dubine pokazuju najjači utjecaj amplitude (otprilike 200 – 267 % varijacije), zatim slijede koeficijent amplitude (otprilike 85 %) i efektivni kut magnetizacije (otprilike 63 %), dok kut nagiba rasjeda pokazuje minimalnu osjetljivost amplitude (otprilike 5 %). Analiza efektivnoga kuta magnetizacije pokazala je njegovu ključnu ulogu u identificiranju optimalnih početnih područja za stabilne procjene, pri čemu lokacija tih područja ovisi o stanju drugih parametara. U primjeni stvarnih podataka hibridna metoda dala je parametre u skladu s vjerojatnim geološkim modelima područja. Rezultati ove studije nude praktičan okvir za poboljšanje inverzije magnetskih podataka, posebno u okruženjima kontaminiranim šumom. U ovoj studiji predstavljen je hibridni pristup koji kombinira Luus-Jaakolin (LJ) i Levenberg-Marquardtov (LM) algoritam za procjenu geometrijskih i fizičkih parametara 2D rasjednih struktura iz magnetnih podataka. Metoda iskorištava mogućnost globalnoga pretraživanja LJ-a i brzu konvergenciju LM-a, a istovremeno uključuje strategiju višestrukoga pokretanja i kontrolirane perturbacije kako bi se prevladala ovisnost o početnoj vrijednosti i nestabilnost kritičnih parametara kao što je efektivni kut nagiba (α). Performanse su procijenjene korištenjem sintetičkih i stvarnih podataka. Za sintetičke podatke s 15 % šuma hibridna metoda postigla je RMS od 4,45 nT, znatno nadmašujući samostalni LJ (17,44 nT) i LM (4,60 nT), a istovremeno je smanjila pogrešku procjene α s 25,40 % na 9,39 % kontroliranom perturbacijom. Kada se primijeni na stvarne magnetske podatke iz bazena Perth u Australiji, hibridni pristup dao je RMS od 1,33 nT u usporedbi s 2,16 nT (LJ) i 10,61 nT (LM), što rezultira parametrima u skladu s vjerojatnim geološkim modelom područja. Ti nalazi pokazuju da hibridni okvir nudi vrhunsku točnost i stabilnost za inverziju magnetskih podataka, posebno u uvjetima šuma.

Ključne riječi:
magnetska inverzija, rasjed, Luus-Jaakolin algoritam, Levenberg-Marquardtov algoritam, hibridni Luus-Jaakola-Levenbergov algoritam

Author's contribution

Mojtaba Babaei (Assistant Professor of Geophysics): conceptualisation, methodology, investigation, software, validation, writing – original draft, and writing – review and editing. **Mohammad Rezaie** (Assistant Professor of Geophysics): data curation, formal analysis, visualisation, and review and editing.
All authors have read and agreed to the published version of the manuscript.